An Optimized *in situ* Quantification Method of Leaf H$_2$O$_2$ Unveils Interaction Dynamics of Pathogenic and Beneficial Bacteria in Wheat

Pablo Carril[1,2], Anabela Bernardes da Silva[2], Rogério Tenreiro[2] and Cristina Cruz[1]*

[1] Plant-Soil Ecology Laboratory, Center for Ecology, Evolution and Environmental Changes (CE3C), Faculty of Sciences, University of Lisbon, Lisbon, Portugal, [2] BioISI – Biosystems and Integrative Sciences Institute, Faculty of Sciences, University of Lisbon, Lisbon, Portugal

Hydrogen peroxide (H$_2$O$_2$) functions as an important signaling molecule in plants during biotic interactions. However, the extent to which H$_2$O$_2$ accumulates during these interactions and its implications in the development of disease symptoms is unclear. In this work, we provide a step-by-step optimized protocol for *in situ* quantification of relative H$_2$O$_2$ concentrations in wheat leaves infected with the pathogenic bacterium *Pseudomonas syringae* pv. *atrofaciens* (*Psa*), either alone or in the presence of the beneficial bacterium *Herbaspirillum seropedicae* (RAM10). This protocol involved the use of 3-3′diaminobenzidine (DAB) staining method combined with image processing to conduct deconvolution and downstream analysis of the digitalized leaf image. The application of a linear regression model allowed to relate the intensity of the pixels resulting from DAB staining with a given concentration of H$_2$O$_2$. Decreasing H$_2$O$_2$ accumulation patterns were detected at increasing distances from the site of pathogen infection, and H$_2$O$_2$ concentrations were different depending on the bacterial combinations tested. Notably, *Psa*-challenged plants in presence of RAM10 accumulated less H$_2$O$_2$ in the leaf and showed reduced necrotic symptoms, pointing to a potential role of RAM10 in reducing pathogen-triggered H$_2$O$_2$ levels in young wheat plants.

Keywords: hydrogen peroxide (H$_2$O$_2$), biotic interactions, image processing, color deconvolution, 3-3′diaminobenzidine (DAB)

INTRODUCTION

Accumulation of reactive oxygen species (ROS) is a common plant response to pathogens, having many and often contrasting functions depending on the plant-pathogen system under study (González-Bosch, 2018). Any type of ROS has specific biochemical characteristics and most of them are extremely unstable (Mittler, 2017). However, hydrogen peroxide (H$_2$O$_2$)

Abbreviations: AUC, area under curve; DAB, 3,3′-diaminobenzidine; *Psa, Pseudomonas syringae* pv. *atrofaciens* strain 2213; RAM10, *Herbaspirillum seropedicae* strain RAM10; ROI, region of interest; SDW, sterile deionized water.

is relatively more stable having a half-life time of more than 1 ms, and is considered the predominant ROS involved in cellular signaling (Černý et al., 2018). ROS regulate numerous immune responses to invading microorganisms, including both the hypersensitive and programmed cell death responses, the cross-linking of cell wall proteins, the deposition of callose or the activation of redox-sensitive genes. Furthermore, ROS, participate in cell-to cell signal transduction to systemic tissues, where localized ROS bursts can induce defenses to prepare (or "prime") plants for future challenges (Torres et al., 2006; Noctor et al., 2018).

Changes in ROS levels also occur during beneficial interactions. Upon contact with plant growth promoting rhizobacteria (PGPR), plant H_2O_2 levels often increase, and H_2O_2 accumulation can be primed for enhanced resistance against pathogens (Ahn et al., 2007). Notably, PGPR can alleviate oxidative stress by modifying the activity of antioxidant enzymes and by modulating H_2O_2 concentrations in the leaf (Lucas et al., 2014; García-Cristobal et al., 2015; Singh and Jha, 2017). As a consequence, PGPR have emerged as a promising alternative to increase oxidative stress tolerance and disease resistance in plants (Islam et al., 2014; Pieterse et al., 2014). Wheat (*Triticum aestivum*) is challenged by several bacterial pathogens, which can cause severe diseases and pests (Valencia-Botín and Cisneros-López, 2012). The pathogen *Pseudomonas syringae* pv. *atrofaciens* (*Psa*) can infect wheat leaves and cause longitudinal brown necrotic-like lesions in the in the site of pathogen entrance resembling those occurring during oxidative stress as a result of high accumulation of ROS in the infection point (Duveiller, 1997).

Despite oxidative stress and pathogen responses are well-studied processes involving H_2O_2 in various ways, it is unclear how H_2O_2 signaling operates in the presence of both pathogenic and beneficial bacteria. This study aims to provide an optimized protocol for *in situ* detection and quantification of relative H_2O_2 concentrations in wheat leaves bacterized with pathogenic and beneficial bacteria, both individually or in combination. This was achieved by combining the 3-3′diaminobenzidine (DAB) staining method previously used for plant material (Wang et al., 2007) and image processing with Fiji/ImageJ software. The combination of these techniques enabled the application of a linear regression model correlating the intensity of the pixels resulting from DAB staining with a given concentration of H_2O_2. This model was suitable for detection and quantification of relative H_2O_2 accumulation in different leaf areas upon infiltration with *Psa* and root-inoculation with the PGPR *Herbaspirillum seropedicae* strain RAM10, either individually or in combination. Furthermore, the area of the lesion caused by *Psa* was measured in presence or absence of previous root-inoculation with RAM10.

This method was suitable to analyze and compare the differential H_2O_2 induction effect between the experimental conditions tested. Our results show that H_2O_2 accumulates at different degrees depending on the leaf region or the different plant-bacteria interactions. Notably, *Psa*-challenged plants in presence of RAM10 showed reduced H_2O_2 accumulation as well as less necrotic symptoms in the leaf, suggesting a PGPR-mediated reduction in oxidative stress levels upon pathogen challenge.

MATERIALS AND METHODS

Bacterial Growth Conditions
Herbaspirillum seropedicae strain RAM10 (RAM10), isolated from *Graminaceae* plants (Olivares et al., 1996), was grown in DYGS medium (composition g L^{-1}: 2.0 glucose; 2.0 malic acid; 2.0 yeast extract; 1.5 peptone; 0.5 K_2HPO_4; 0.5 $MgSO_4$ $7H_2O$; 1.5 L-glutamic acid; pH 6.5) at 28°C and 120 rpm, under dark conditions overnight. Bacterial cells collected by centrifugation (2374 × g, 10 min) were washed twice with sterile deionized water (SDW) and resuspended in 1/4 Hoagland solution (Hoagland and Arnon, 1950) to a final OD_{600} = 1 (10^9 CFU/mL) for root inoculation of seedlings.

Pseudomonas syringae pv. *atrofaciens* strain 2213 (*Psa*), isolated from *T. aestivum* plants (McCulloch, 1920) was grown in NB medium (composition g L^{-1}: 10.0 tryptone; 5.0 meat extract; 5.0 NaCl) at 28°C and 120 rpm, under dark conditions overnight. Bacterial cells collected by centrifugation (2374 × g, 10 min) were washed twice and resuspended in SDW to a final density of 10^9 CFU/mL for pressure infiltration into the leaves.

Plant Growth Conditions
Wheat (*Triticum aestivum* cultivar "Trigo mole") seeds were surface-sterilized (1.5 min 70% ethanol; 1× wash in SDW; 3 min NaOCl; 10× wash in SDW), soaked for 12 h in SDW and heat-treated (10 min, 50°C; 1 mL/seed). Seeds were then aseptically transferred to square Petri dishes (20 seeds per dish) containing 1.5% water agar and incubated at 30°C in dark conditions for 48 h and kept in a growing chamber with a 16/8 h light/dark photoperiod, temperature 25/20°C and relative humidity (RH) 70%/50%), for 48 h. Four day-old seedlings were then transferred to empty tip boxes containing 225 mL of 1/4 Hoagland solution, with the leaves emerging from the holes of the rack and the Hoagland solution bathing the roots.

Measurement of Leaf Symptoms
Four day-old seedlings were divided in four groups (four tip boxes) composed of 7 seedlings each, with three replicates per group: control, non-bacterized (C); RAM10-inoculated (RAM10); *Psa*-infiltrated (*Psa*) and both RAM10-inoculated and *Psa*-infiltrated (RAM10 + *Psa*). In both RAM10 and RAM10 + *Psa* groups, 25 mL of RAM10 suspension was added to the Hoagland solution bathing the roots to a final density of 10^8 CFU/mL (250 mL final Hoagland volume). Each box was then sealed in plastic gas exchange bags. Four days after RAM10 inoculation, *Psa* and RAM10 + *Psa* groups were pressure infiltrated in the central part of the leaf with 1 mL of *Psa* culture using a needless syringe. Leaves of C and RAM10 groups were pressure infiltrated with 1 mL of SDW. Five days after infiltration, leaves were cut, mounted in transparent plastic slides and pictures were taken. The area of both necrotic and chlorotic symptoms was quantified from the digitalized images using the image processing software Fiji/ImageJ (ImageJ, RRID:SCR_003070).

For this, the affected area was manually defined using both the "polygon" selection tool and the "brush" tool to adjust the size of the selection to the shape of the affected area. The size of the affected area was expressed as mm^2 of both necrotic and chlorotic symptoms.

Construction of DAB-H$_2$O$_2$ Calibration Curve: Step-by-Step Protocol

(1) Prepare several H$_2$O$_2$ dilutions $\leq$ 47 mM from stock solution at 30% (w/w), that is 9.8 M, with ultra-pure water or sterile deionized water (SDW).

- Note: H$_2$O$_2$ Molar mass = 34.01468 g mol^{-1}, density = 1.11 g mL^{-1}.

(2) Measure the absorbance of the H$_2$O$_2$ dilutions at 240 nm in a quartz cuvette, after adjusting zero absorbance with the water used for dilutions.

(3) Calculate the exact H$_2$O$_2$ concentration of the different solutions using Lambert-Beer law, considering the molar attenuation coefficient or absorptivity (ε) for H$_2$O$_2$ at 240 nm equal to 42.3 M^{-1} cm^{-1} and pathlength (l) = 1 cm.
Note: Lambert-Beer law is valid up to an absorbance $\leq$2.

(4) Prepare paper filter disks with an area $\leq$internal area of a 2 mL microtube. Place the disk inside de microtube in horizontal position.

Impregnate all the disk surfaces with adequate volume of H$_2$O$_2$ solution, without overloading, and add the DAB solution (1 mg/mL). Make this in triplicate for each [H$_2$O$_2$]. Additionally, place 3 disks with DAB only for later background subtraction.

Note: It is important to avoid overloading of paper filter disks, since the precipitated formed by H$_2$O$_2$ reaction with DAB may sediment in the bottom of the microtube, underestimating [H$_2$O$_2$] and subsequent analysis. We used filter disks with a diameter of 55 mm, 16.6 μL of H$_2$O$_2$ solution and 150 μL DAB per disk.

(5) Incubate the microtubes at room temperature and in dark conditions, overnight.

(6) Take out the disks with clean tweezers and mount the disks in a transparent plastic slide.

(7) Digitalize the disks with a scanner and open the image with Fiji/ImageJ software.

- Apply the color deconvolution plugin in order to unmix the color vectors of the digitalized disks. From the resulting panel containing DAB color only, select each disk (region of interest, ROI) using the "oval" selection tool and measure the initial average DAB pixel intensity (*ii*), expressed as:
- $ii = \frac{\sum \text{vpx}}{\text{n°px}}$
- where *ii* is the initial average pixel intensity; $\sum$vpx is the sum of the values of the pixels composing the selected area; and n°px is the number of pixels composing the selected area.

(8) Invert the initial average pixel intensity values by using the formula:

- $iinv = 255 - ii$
- being *iinv* the inverted average pixel intensity. Note that, for 8-bit images, *i* ranges from 0 (zero = deep brown, highest expression), to 255 (total white).

(9) Subtract the background DAB intensity to the *iinv* values, according to the formula:

- $ifinal = iinv - iblank$
- where *ifinal* is the final intensity of the disk and *iblank* is the average intensity value of 3 filters drenched with DAB only.

(10) Construct a calibration curve correlating the *ifinal* values with the corresponding H$_2$O$_2$ concentration (μmol H$_2$O$_2$/cm^2). Calibration curves with average values (based on triplicates) are presented in **Figure 2A**.

(11) Quantify average pixel intensity also in the complimentary image and represent in a graph the values of average pixel intensity with the corresponding H$_2$O$_2$ concentration (μmol H$_2$O$_2$/cm^2) (**Supplementary Figures 1A,B**).
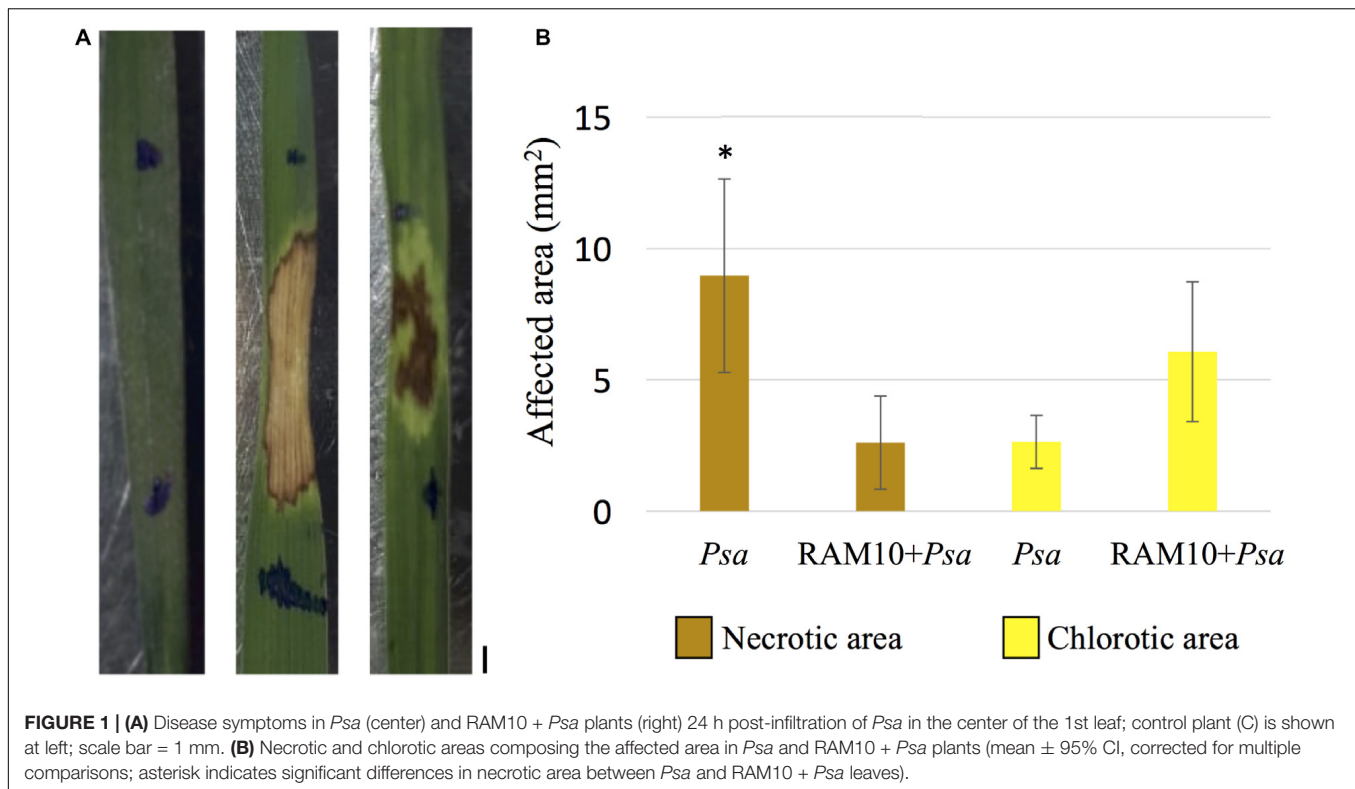
Quantification of Relative H$_2$O$_2$ Concentration in Leaves Using 3,3-Diaminobenzidine (DAB)

Ten seedlings from each of the four treatments (C, *Psa*, RAM10 + *Psa*) were grown to detect H$_2$O$_2$ accumulation in the 1st leaf. Detection of H$_2$O$_2$ in leaves was carried out using the 3,3-diaminobenzidine (DAB) staining method already used for barley and wheat plants (Thordal-Christensen et al., 1997; Wang et al., 2007), with slight modifications: 1, 2, 6, 24, and 48 h post-inoculation (hpi), leaves were cut and the cut ends were immersed in 1 mL of a solution containing 1 mg/mL DAB dissolved in HCl-acidified (pH 3.8) SDW. Leaves were incubated in a growing chamber overnight to allow DAB uptake and reaction with H$_2$O$_2$. Solutions were kept under dark conditions.

After incubation, leaves were decolorized in boiling ($\sim$78°C) 95% ethanol for 20 min and transferred into a solution containing water and 20% glycerol.

Leaf segments were placed in filter paper to remove the excess of glycerol solution, mounted in transparent plastic slides, scanned (Epson XP-235) and the images opened with Fiji/ImageJ software. Initial settings of the software were applied to measure area (mm^2) and mean pixel intensity. Global scale of the image analysis was set as 46.5 pixels = 1 mm. Then, the image was submitted to the plug-in "color deconvolution" using the built-in vector HDAB in order to limit to the DAB dye image. Three different areas (regions of interest, ROIs) were selected for analysis in the DAB only image: from 0 to 4, from 4 to 8 and from 8 to 12 mm from the *Psa* infiltration site. Selection of ROIs was performed using the "rectangle" selection tool. Once the three areas were selected, the "brush" tool was used to adjust the size of the rectangle according to the leaf shape. Then, the area in mm^2 and the mean intensity of DAB was calculated. Intensity values ranged from 0 (deep brown) to 255 (total white).

The average DAB intensity was calculated according to the formula: i$_{DAB}$ = 255-i, being i$_{DAB}$ = final DAB intensity of the

FIGURE 1 | (A) Disease symptoms in *Psa* (center) and RAM10 + *Psa* plants (right) 24 h post-infiltration of *Psa* in the center of the 1st leaf; control plant (C) is shown at left; scale bar = 1 mm. **(B)** Necrotic and chlorotic areas composing the affected area in *Psa* and RAM10 + *Psa* plants (mean ± 95% CI, corrected for multiple comparisons; asterisk indicates significant differences in necrotic area between *Psa* and RAM10 + *Psa* leaves).

ROI compared to average intensity of total white of the ROI, i = the mean DAB intensity of the ROI. In order to subtract the background of the leaf tissue, the average intensity of 20 leaves pressure-infiltrated with water, incubated in water without DAB, and then destained (blank leaves) was measured and subtracted to the i_{DAB} value calculated for each ROI, according to the formula: $f_{DAB} = i_{DAB} - i_{blank}$, being f_{DAB} = final DAB intensity and i_{blank} the average intensity of the blank leaves.

RESULTS

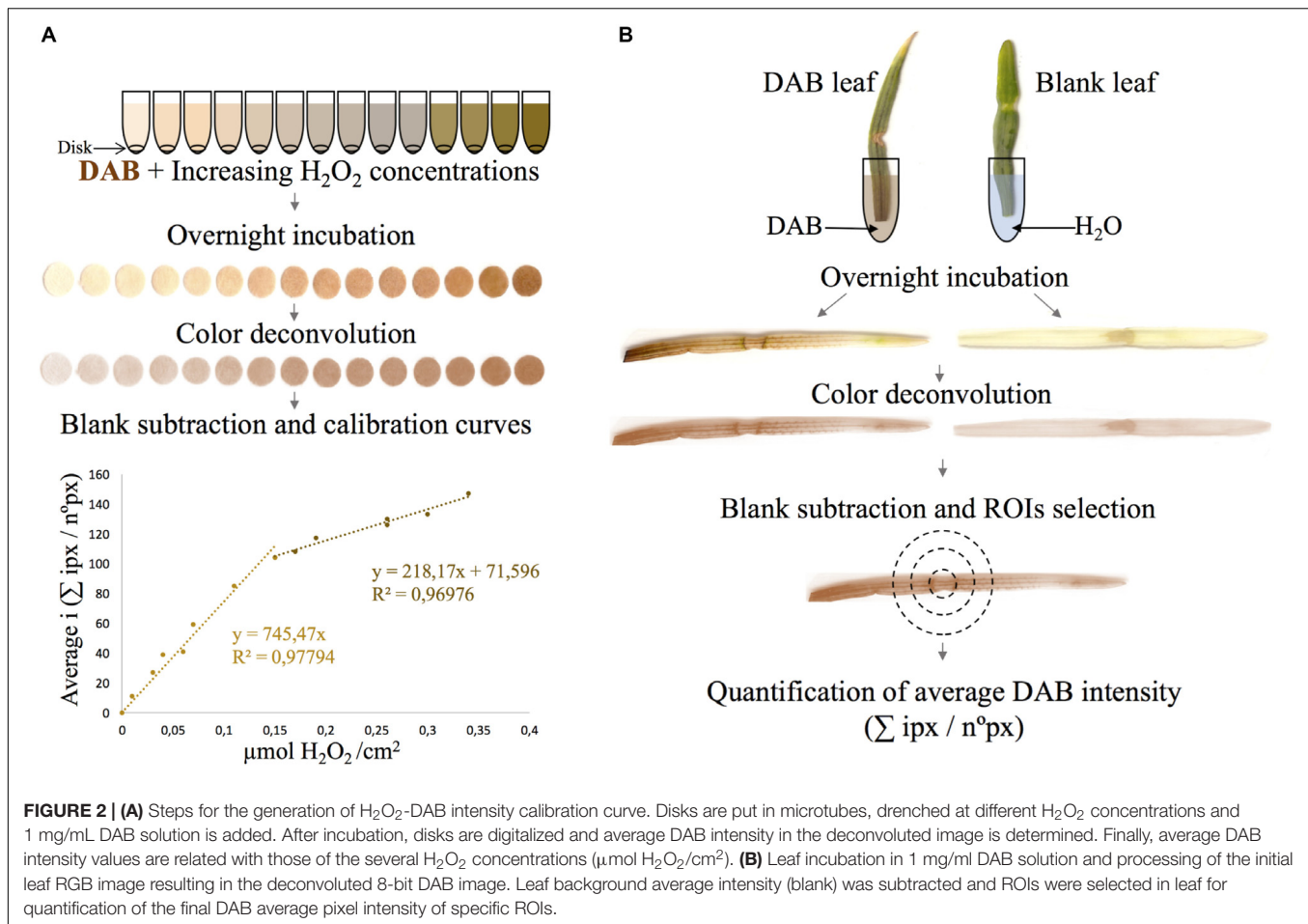### *Psa*-Triggered Disease Symptoms in Absence or Presence of RAM10

Infiltration with *Psa* in wheat leaves caused the development of dried brown, necrotic lesions surrounded by chlorosis after 24 h both in *Psa* and RAM10 + *Psa* seedlings (**Figure 1A**). Despite both diseased leaf areas being similar in size, the proportion of chlorotic and necrotic symptoms was different between the two treatments (**Figure 1B**). Around 75% of the diseased leaf area in *Psa* leaves was composed of necrotic tissue, which appeared in form of a dried brown area, presumably as a result of the onset a hypersensitive response at the site of pathogen entrance. This necrotic area often reached the borders of the leaf and was surrounded by a thin layer of chlorotic symptoms. Average necrotic area in RAM10 + *Psa* leaves was significantly reduced compared to *Psa* ones, with 30% of the total diseased leaf area showing necrosis, and with chlorosis representing most of the total diseased area.

Regression Model for H_2O_2 Quantification

A linear regression model to quantify H_2O_2 was applied by combining the DAB staining method with image processing using Fiji/ImageJ software. This was done by relating average DAB intensity values to a given amount of H_2O_2. A DAB color gradient was generated by incubating filter disks in separate microtubes containing DAB + increasing H_2O_2 concentrations. Disks ranged from light to dark-brown stained disks, relative to low to high H_2O_2 concentrations (or low to high intensities), respectively (**Figure 2A**). Disks were digitalized and subjected to the color deconvolution plugin, allowing the separation of the initial RGB image into three 8-bit images, which corresponded to the three vector colors composing the image, being: (1) the brown vector, used for subsequent H_2O_2 quantification; (2) the blue vector, not present in the DAB stained disk and (3) a residual channel, also referred to as the complimentary vector, containing the complementary of the other color(s).

Two calibration curves were constructed relating the average DAB intensity values obtained in the DAB only stained section with the corresponding H_2O_2 concentration (μmol H_2O_2/cm^2) applied. The first curve ranged from 0 to 104 DAB intensity values and the second one from 104 to 147 values. Both curves showed a linear relationship between the two variables ($R^2 \geq 0.97$; **Figure 2A**).

Previous authors have stressed the importance of taking into account the intensity values of the pixels in the complimentary image, since they may contain shades of DAB, leading to false positive stain separation (Ruifrok and Johnston, 2001;

FIGURE 2 | (A) Steps for the generation of H_2O_2-DAB intensity calibration curve. Disks are put in microtubes, drenched at different H_2O_2 concentrations and 1 mg/mL DAB solution is added. After incubation, disks are digitalized and average DAB intensity in the deconvoluted image is determined. Finally, average DAB intensity values are related with those of the several H_2O_2 concentrations (μmol H_2O_2/cm^2). **(B)** Leaf incubation in 1 mg/ml DAB solution and processing of the initial leaf RGB image resulting in the deconvoluted 8-bit DAB image. Leaf background average intensity (blank) was subtracted and ROIs were selected in leaf for quantification of the final DAB average pixel intensity of specific ROIs.

Varghese et al., 2014). In order to correct the intensity values in the DAB only vector, the pixel intensity of the same disks in the complimentary vector was quantified (**Supplementary Figure 1A**), and a curve relating the average green intensity values versus μmol H_2O_2/cm^2 was plotted (**Supplementary Figure 1B**). However, contrary to the DAB only vector, the average intensity values of each disk were not proportional to the applied H_2O_2 concentration. In fact, several filters with higher H_2O_2 concentrations were less stained compared to those drenched with DAB solution only, indicating that average intensity in the complimentary image did not depend on H_2O_2 concentration. Because summing these values would decrease the accuracy of H_2O_2 quantification, average intensity values in the complimentary image were not considered.
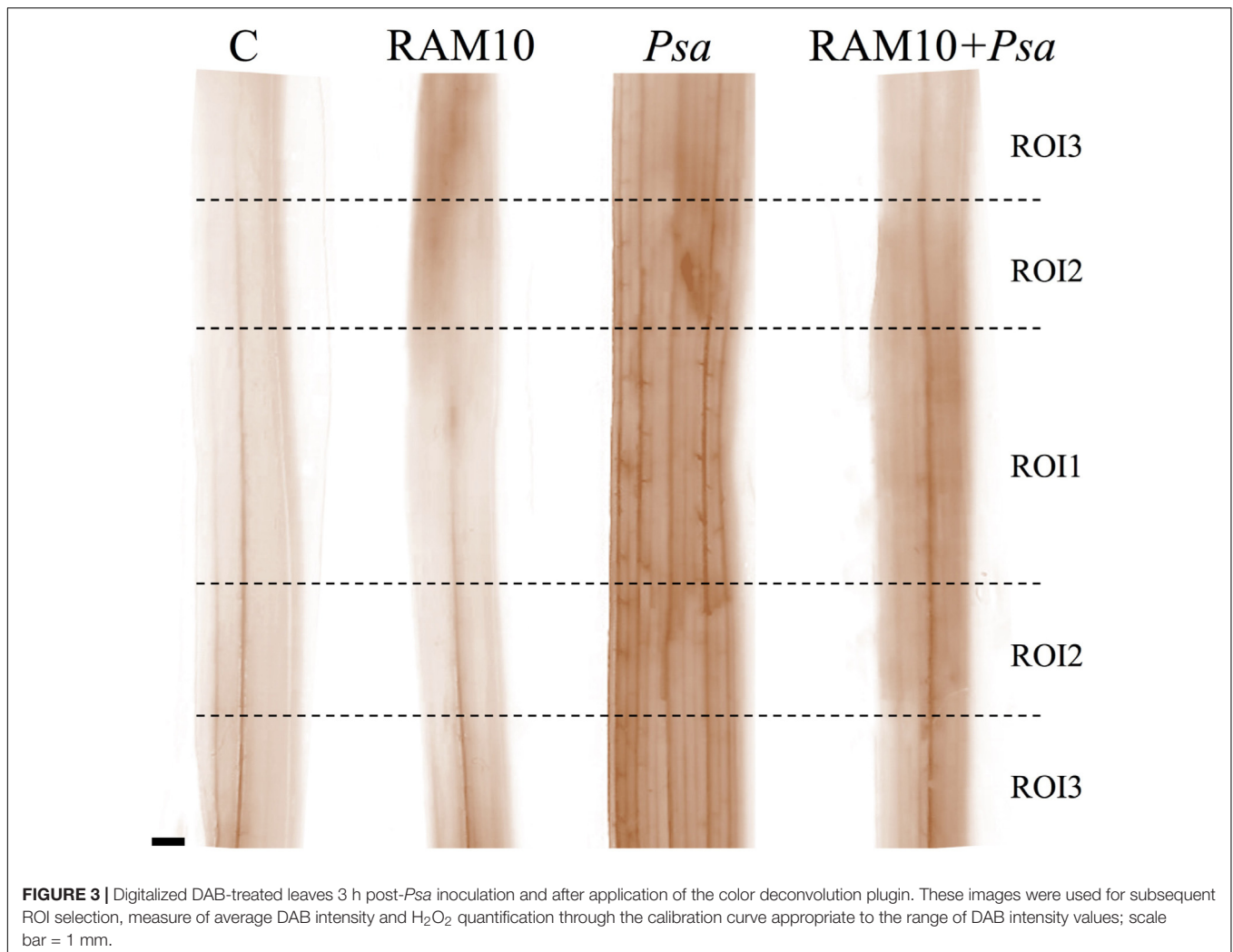
Determination of H_2O_2 Accumulation in Leaves

In parallel, wheat leaves were incubated in the DAB solution, digitalized and subjected to the color deconvolution plugin (**Figure 2B**). DAB color was visualized, and different ROIs were selected to measure the average DAB intensity and determine relative H_2O_2 concentration using the calibration curve. Accumulation of H_2O_2 was visualized as dark-brown

precipitates resulting from the oxidation of DAB by H_2O_2 present in the leaf. A more intense staining was observed in the vascular beams (**Figure 3**).

Infiltration of *Psa* induced an active production of H_2O_2 in the leaf, both upwards and downwards from the site of infection. Pathogen-infiltrated treatments (*Psa* and RAM10 + *Psa*) showed increased H_2O_2 accumulation in the whole selected leaf area ($\sum$ROIs, **Figure 4**) compared to both C and RAM10 ones. This increase was always more pronounced in *Psa* treatment, compared to which RAM10 + *Psa* plants accumulated significantly less H_2O_2. RAM10 treatments showed similar H_2O_2 accumulation relative to C ones, indicating that root inoculation of RAM10 did not have a significant H_2O_2 induction effect in aboveground tissues.

The analysis of each independent ROI (**Figure 4**) showed that H_2O_2 is produced at different degrees in the leaf, decreasing its accumulation at increasing distances from the infiltration point. After 6 h of *Psa* inoculation, both challenged treatments reached maximum H_2O_2 accumulation in ROI1 (1.39 and 1.18 μmol/cm^2 H_2O_2 in *Psa* and RAM10 + *Psa* plants, respectively), which was covered by dried-brown necrotic tissue 24 hpi. Also, in ROI2 and ROI3, H_2O_2 levels were always higher in *Psa* plants compared to RAM10 + *Psa* ones, showing significant differences at 24 and 48 hpi.

FIGURE 3 | Digitalized DAB-treated leaves 3 h post-*Psa* inoculation and after application of the color deconvolution plugin. These images were used for subsequent ROI selection, measure of average DAB intensity and H$_2$O$_2$ quantification through the calibration curve appropriate to the range of DAB intensity values; scale bar = 1 mm.

In order to assess the RAM10-mediated alleviation effect, the area under curve (AUC) of H$_2$O$_2$ accumulation was calculated at each time post-infection in the different treatments, and the evolution of cumulative H$_2$O$_2$ fold induction triggered by *Psa* was analyzed for the AUC ratios *Psa*/RAM10 and (RAM10 + *Psa*)/RAM10 (i.e., the H$_2$O$_2$ induction effect of *Psa* in presence or absence of RAM10 relative to RAM10-only inoculated seedlings; **Figure 5**, bars), as well as for the *Psa*/(RAM10 + *Psa*) AUC ratio (i.e., the H$_2$O$_2$ induction effect of *Psa* in absence of RAM10 relative to RAM10 + *Psa* seedlings; **Figure 5**, black lines).
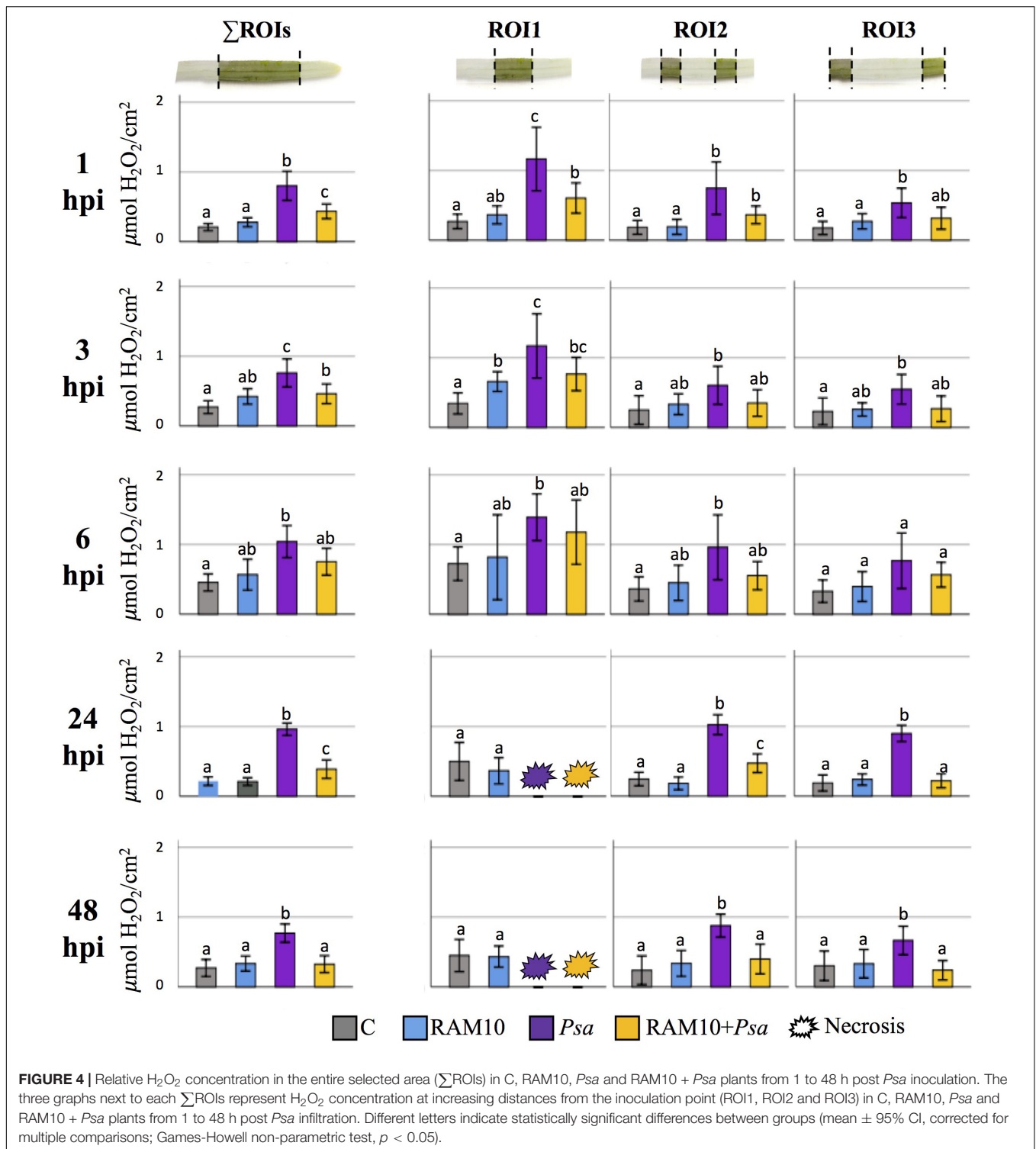
Psa-triggered H$_2$O$_2$ induction effect was always reduced when the pathogen was inoculated in presence of RAM10. This RAM10-mediated alleviation of H$_2$O$_2$ accumulation was evident in all timepoints, where *Psa* plants accumulated between 1.5 and 2-fold more H$_2$O$_2$ relative to RAM10 + *Psa* ones along timepoints. In ROI3, while H$_2$O$_2$ accumulation in *Psa* plants increased at 24 and 48 hpi, it remained unchanged in RAM10 + *Psa* ones, highlighting a statistically significant alleviation effect of H$_2$O$_2$ accumulation in this region at 24 and 48 hpi (black line, **Figure 5**). These results

point that PGPR-inoculated plants may be more sensitive to H$_2$O$_2$ signaling, not requiring its massive accumulation upon a challenge.

DISCUSSION

Detection of H$_2$O$_2$ by DAB Staining Coupled With Imaging Software Analysis
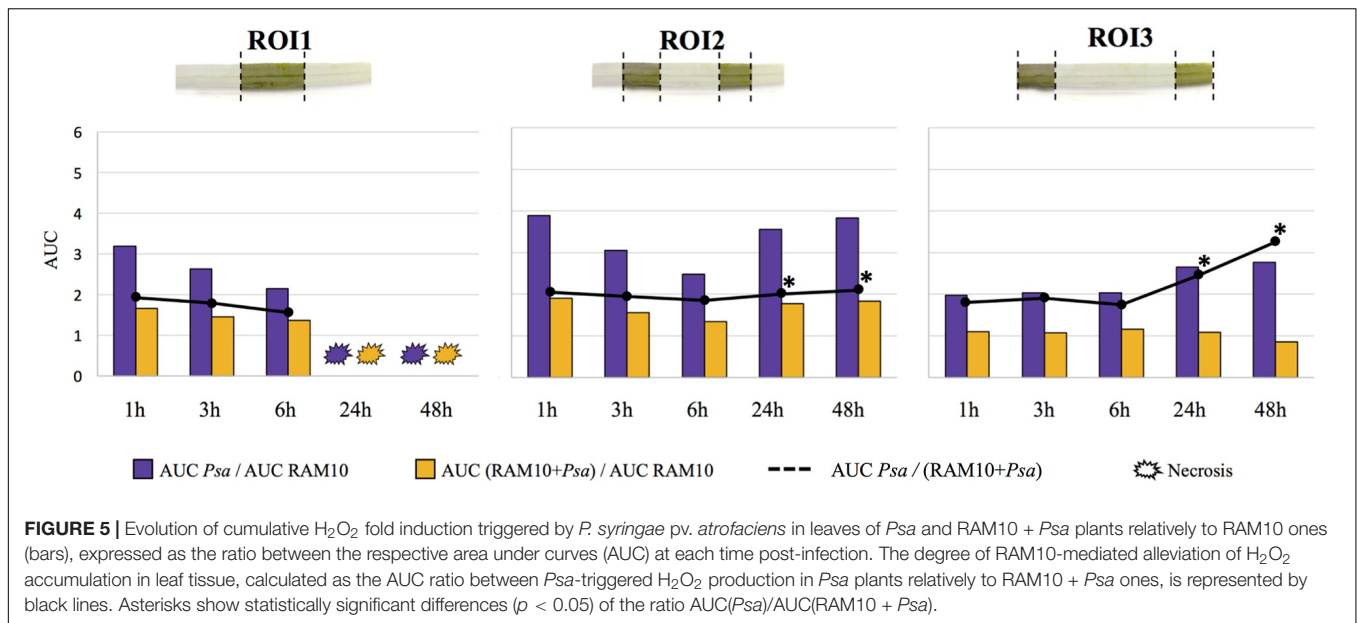
There exist numerous functions accounted to H$_2$O$_2$ in response to pathogens. Despite its crucial role in plant metabolism, there is little consensus regarding the amount of H$_2$O$_2$ dynamics in plants challenged with pathogens and pre-treated with PGPR. This is mainly due to both biological variability and technical inaccuracies during its quantification (Queval et al., 2008). Various techniques can quantify H$_2$O$_2$ contents in plant tissue extracts, such as those relying on absorbance of oxidized products with altered spectral characteristics (Junglee et al., 2014) or on light emission as fluorescence or luminescence (Miller et al., 2012). Enzymatic assays or the use of metal catalysts of H$_2$O$_2$-dependent reactions are also widely used, both of which can

FIGURE 4 | Relative H$_2$O$_2$ concentration in the entire selected area ($\sum$ROIs) in C, RAM10, *Psa* and RAM10 + *Psa* plants from 1 to 48 h post *Psa* inoculation. The three graphs next to each $\sum$ROIs represent H$_2$O$_2$ concentration at increasing distances from the inoculation point (ROI1, ROI2 and ROI3) in C, RAM10, *Psa* and RAM10 + *Psa* plants from 1 to 48 h post *Psa* infiltration. Different letters indicate statistically significant differences between groups (mean ± 95% CI, corrected for multiple comparisons; Games-Howell non-parametric test, *p* < 0.05).

overcome problems of H$_2$O$_2$ specificity (Queval et al., 2008; Nagaraja et al., 2009). However, some of the challenges that these techniques face include (1) complex interactions between metals or enzymes that may occur during the extraction rather than in the intact tissue, (2) H$_2$O$_2$ dilution effects at increasing amount of leaf tissue extracted, which may often mask the real H$_2$O$_2$

response (Queval et al., 2008), (3) manipulation effects during sample preparation.

Image analysis for *in situ* quantification of DAB staining has the advantage over biochemical assays that it is non-destructive and minimizes the manipulation of plant material. Furthermore, DAB staining method relies on the activity of peroxidases present

FIGURE 5 | Evolution of cumulative H$_2$O$_2$ fold induction triggered by *P. syringae* pv. *atrofaciens* in leaves of *Psa* and RAM10 + *Psa* plants relatively to RAM10 ones (bars), expressed as the ratio between the respective area under curves (AUC) at each time post-infection. The degree of RAM10-mediated alleviation of H$_2$O$_2$ accumulation in leaf tissue, calculated as the AUC ratio between *Psa*-triggered H$_2$O$_2$ production in *Psa* plants relatively to RAM10 + *Psa* ones, is represented by black lines. Asterisks show statistically significant differences (p < 0.05) of the ratio AUC(*Psa*)/AUC(RAM10 + *Psa*).

in the leaf, not requiring addition of external peroxidases, which may be another factor affecting ideal *in vivo* conditions. In this work, we presented an optimized *in situ* detection method using DAB staining coupled to image processing to both detect and quantify H$_2$O$_2$ in leaves.

DAB stained leaves can be digitalized, opened in Fiji/ImageJ and subjected to the color deconvolution plugin, an algorithm developed by Ruifrok and Johnston (2001), which unmixes the color information of the digitalized leaf. The color deconvolution plugin has been previously used for human tissue microscopy analysis (Lessey and Savaris, 2013; Varghese et al., 2014). In this work, this method was adapted for young wheat leaves and used to detect the spatial distribution of the DAB intensity at increasing distances from the infection site. As a result, an image with DAB only staining is generated, and the average intensity of its pixels can be quantified after the selection of specific ROIs. Having DAB stained leaves digitalized, other ROIs can be defined anytime.

In previous studies using DAB staining, leaf H$_2$O$_2$ content was estimated as the percentage of dark brown DAB pixels relative to the pixels composing the leaf area. In order to express H$_2$O$_2$ content in concentration units, these studies relied on parallel spectrophotometric assays for H$_2$O$_2$ quantification (Luna et al., 2011; Liu et al., 2014; Wu et al., 2019). However, these analyses require the involvement of different plant samples for both the DAB staining and the spectrophotometry, since the DAB signal could not directly correlate with specific H$_2$O$_2$ concentration units. In the present study, the application of a linear model combining average pixel intensity values with known H$_2$O$_2$ concentrations allowed to quantify relative H$_2$O$_2$ concentrations in the leaf according to its DAB staining intensity values. The generation of this curve avoided the manual setting of a maximum and minimum threshold intensities in the images, which can itself be subjective, leading to misinterpretations in tissue sample scoring (Varghese et al.,

2014). It was neither necessary to linearize the intensity values to OD values, as indicated by previous articles (Ruifrok and Johnston, 2001; Varghese et al., 2014), since the values of DAB intensity were linearly related with the concentrations of H$_2$O$_2$ and can therefore be used for extrapolating H$_2$O$_2$ concentration from DAB intensity values. Furthermore, the H$_2$O$_2$ dilution effects were minimized by selecting small (8 mm) ROIs in intact (stressed or non-stressed) leaves after image processing. Manipulation of the plant material was almost inexistent, since the only stress applied to the plant was an initial cut at the base of the cotyledon, immediately prior to DAB incubation. Considering this, specific ROIs were selected excluding both the basal part of the leaf and its apex, which, in few cases, started to senesce (data not shown).

Application of the New Method for Studying Biotic Interactions

Leaves infiltrated with *Psa* accumulated H$_2$O$_2$ both locally and at further distances from the infection point, where dark brown DAB precipitates were found to be more intense in the vascular beams. Tissue-specific localization of H$_2$O$_2$ associated with vascular tissues has been previously observed (Ślesak et al., 2007) and is in agreement with previous studies which suggest that vascular bundles can synthesize these ROS signals during stress for rapid autopropagation and induction of systemic stress immunity (Libik-Konieczny et al., 2015; Gaupels et al., 2017).

The method proposed in this study was applicable to analyze and compare the differential H$_2$O$_2$ induction effect of *Psa* in the presence or absence of the PGPR RAM10. H$_2$O$_2$ accumulated at higher levels in the site of pathogen entrance (ROI1), which became necrotic 24 hpi. These observations suggest that induction of hypersensitive cell death by *Psa* in the site of

infection is temporally preceded by H_2O_2 accumulation in the site of pathogen entry, while H_2O_2 accumulation, but not cell death, was induced in the tissue adjacent to the infiltration point. Since ROS participate in cell-to cell signal transduction to systemic tissues, this ROS accumulation in distant parts from the pathogen entry could be a source of signals for establishment of further defenses to prepare (or "prime") plants for future challenges (Noctor et al., 2018).

Interestingly, RAM10-treated plants showed consistently less H_2O_2 accumulation, where the most remarkable alleviation effect was observed 24 and 48 hpi in the most distal area (ROI3), which maintained a low, initial *Psa*-induced H_2O_2 accumulation overtime. These observations suggest that necrosis and H_2O_2 signal propagation occurs in both *Psa* and RAM10 + *Psa* plants, but RAM10-inoculated plants can alleviate the degree of H_2O_2 accumulation upon *Psa* challenge and maintain the basal levels of stress initially triggered by *Psa* in more distal parts of the leaf, without undergoing a further H_2O_2 accumulation. This reduction in ROS levels in challenged plants pre-inoculated with a beneficial microorganism, including bacteria and fungi, has been previously observed. For example, endophytic bacteria-primed *Abelmoschus esculentus* plants expressed lower level of H_2O_2 accumulation upon *Sclerotium rolfsii* challenge, compared to unprimed plants, probably due to the enhanced expression of antioxidant enzymes (Ray et al., 2016). In tobacco leaves, *Bacillus atrophaeus* HAB-5 inhibited ROS accumulation in leaves during TMV infection, which was related with enhanced resistance against the virus and inhibition of cell death (Rajaofera et al., 2020). Besides, the fungus *T. harzianum*–mediated biocontrol may be related to alleviating *Rhizoctonia solani*-induced oxidative stress by reducing the levels of hydroxyl radical, $O_2^{\cdot-}$ and H_2O_2 after pathogen challenge (Singh and Singh, 2011). Furthermore, the pre-treatment of alfalfa plants with lipopolysaccharides from *Sinorhizobium meliloti* suppressed the yeast elicitor-induced oxidative burst reaction (Albus et al., 2001). One hypothesis to explain this alleviation effect is that RAM10 inoculation may induce weak and transient defense-associated changes in ROS signaling upon contact with roots and this signal may be transmitted to aboveground parts of the plant. Contact with RAM10 could pre-activate H_2O_2 signaling in aboveground tissues, avoiding its massive accumulation upon pathogen challenge and increasing plant sensitivity to H_2O_2 signaling. Contrarily, without being alerted by a previous contact with RAM10, pathogen infiltration in *Psa* plants would lead to a massive, uncontrolled accumulation of H_2O_2, resulting in cellular damage and increased necrotic area (Van Breusegem and Dat, 2006). In relation to this, RAM10 could prime plants to increase antioxidant enzyme activity/production upon a future infection.

CONCLUSION

In this work, we report for the first time an integrated protocol that simultaneously allows to detect DAB distribution, to quantify amount of DAB signal in different leaf regions and to relate this signal to a given concentration of H_2O_2. The method is non-expensive and applicable to analyze and compare the differential H_2O_2 induction effects of wheat plants bacterized with both pathogenic and beneficial bacteria.

This methodology allowed to show that the pathogen *Psa* clearly increased H_2O_2 accumulation in infiltrated leaves. On the contrary, both H_2O_2 levels and disease symptoms induced by this pathogen decreased in presence of RAM10, suggesting a role for this PGPR in the alleviation of pathogen-induced oxidative stress and the progression of necrotic symptoms.

DATA AVAILABILITY STATEMENT

The raw data supporting the conclusions of this article will be made available by the authors, without undue reservation.

AUTHOR CONTRIBUTIONS

PC and AS designed the experiments and analyzed the data in the H_2O_2 quantification part. PC, RT, and CC designed the experiments and analyzed the data concerning the biotic interaction part. PC performed the experiments. All researchers contributed to the research and approved the final version of the manuscript.

ACKNOWLEDGMENTS

SUPPLEMENTARY MATERIAL

The Supplementary Material for this article can be found online at: https://www.frontiersin.org/articles/10.3389/fpls.2020.00889/full#supplementary-material

FIGURE S1 | (A) Values of H_2O_2 concentration in the disks quantified in the complementary image, their average pixel intensity values (averages of three disk replicates) and aspect of the filter disks. **(B)** Relationship between average pixel intensity detected in the complimentary image and (±STDEV) and the amount of H_2O_2 per cm^2 of disk.

REFERENCES

Ahn, I. P., Lee, S. W., and Suh, S. C. (2007). Rhizobacteria-induced priming in *Arabidopsis* is dependent on ethylene, jasmonic acid, and NPR1. *Mol. Plant Microbe Interact.* 20, 759–768. doi: 10.1094/MPMI-20-7-0759

Albus, U., Baier, R., Holst, O., Pühler, A., and Niehaus, K. (2001). Suppression of an elicitor-induced oxidative burst reaction in Medicago sativa cell cultures by

Sinorhizobium meliloti lipopolysaccharides. *New Phytol.* 597:606. doi: 10.1046/j.0028-646x.2001.00214.x

Černý, M., Habánová, H., Berka, M., Luklová, M., and Brzobohatý, B. (2018). Hydrogen peroxide: its role in plant biology and crosstalk with signalling networks. *Int. J Mol. Sci.* 19:2812. doi: 10.3390/ijms19092812

Duveiller, E. (1997). *The Bacterial Diseases of Wheat: Concepts and Methods of Disease Management.* Mexico: CIMMYT.

García-Cristobal, J., García-Villaraco, A., Ramos, B., Gutierrez-Mañero, J., and Lucas, J. A. (2015). Priming of pathogenesis related-proteins and enzymes related to oxidative stress by plant growth promoting rhizobacteria on rice plants upon abiotic and biotic stress challenge. *J. Plant Physiol.* 188, 72–79. doi: 10.1016/j.jplph.2015.09.011

Gaupels, F., Durner, J., and Kogel, K. H. (2017). Production, amplification and systemic propagation of redox messengers in plants? The phloem can do it all! *New Phytol.* 214, 554–560. doi: 10.1111/nph.14399

González-Bosch, C. (2018). Free Radical Biology and Medicine Priming plant resistance by activation of redox-sensitive genes. *Free Radic. Biol. Med.* 122, 171–180. doi: 10.1016/j.freeradbiomed.2017.12.028

Hoagland, D., and Arnon, D. (1950). *The Water-Culture Method for Growing Plants Without Soil.* Berkeley, CA: University of California.

Islam, F., Yasmeen, T., Ali, Q., Ali, S., Arif, M. S., Hussain, S., et al. (2014). Influence of *Pseudomonas aeruginosa* as PGPR on oxidative stress tolerance in wheat under Zn stress. *Ecotoxicol. Environ. Saf.* 104, 285–293. doi: 10.1016/j.ecoenv.2014.03.008

Junglee, S., Urban, L., Sallanon, H., and Lopez-Lauri, F. (2014). Optimized assay for hydrogen peroxide determination in plant tissue using potassium iodide. *Am. J. Anal. Chem.* 5, 730–736. doi: 10.4236/ajac.2014.511081

Lessey, B. A., and Savaris, R. F. (2013). Comparison of HSCORE assessment of endometrial (3 integrin subunit expression with digital HSCORE using computerized image analysis (ImageJ). *Anal. Quant. Cytopathol. Histpathol.* 35, 210–216.

Libik-Konieczny, M., Kozieradzka-Kiszkurno, M., Desel, C., Michalec-Warzecha, Ż, Miszalski, Z., and Konieczny, R. (2015). The localization of NADPH oxidase and reactive oxygen species in in vitro-cultured Mesembryanthemum crystallinum L. hypocotyls discloses their differing roles in rhizogenesis. *Protoplasma* 252, 477–487. doi: 10.1007/s00709-014-0692-2

Liu, Y. H., Offler, C. E., and Ruan, Y. L. (2014). A simple, rapid, and reliable protocol to localize hydrogen peroxide in large plant organs by DAB-mediated tissue printing. *Front. Plant Sci.* 5:745. doi: 10.3389/fpls.2014.00745

Lucas, J. A., García-Cristobal, J., Bonilla, A., Ramos, B., and Gutierrez-Manero, J. (2014). Beneficial rhizobacteria from rice rhizosphere confers high protection against biotic and abiotic stress inducing systemic resistance in rice seedlings. *Plant Physiol. Biochem.* 82, 44–53. doi: 10.1016/j.plaphy.2014.05.007

Luna, E., Pastor, V., Robert, J., Flors, V., Mauch-Mani, B., and Ton, J. (2011). Callose deposition: a multifaceted plant defense response. *Mol. Plant Microbe Interact.* 24, 183–193. doi: 10.1094/MPMI-07-10-0149

McCulloch, L. (1920). Basal glumerot of wheat. *J. Agric. Res.* 18, 543–549.

Miller, G., Schlauch, K., Tam, R., Cortes, D., Torres, M. A., Shulaev, V., et al. (2012). The plant NADPH oxidase RBOHD mediates rapid systemic signaling in response to diverse stimuli. *Sci. Signal.* 2:ra45. doi: 10.1126/scisignal.2000448

Mittler, R. (2017). ROS are good. *Trends Plant Sci.* 22, 11–19. doi: 10.1016/j.tplants.2016.08.002

Nagaraja, P., Shivakumar, A., and Shrestha, A. K. (2009). Quantification of hydrogen peroxide and glucose using 3-methyl-2-benzothiazolinonehydrazone hydrochloride with 10, 11-dihydro-5 H-benz (b, f) azepine as chromogenic probe. *Anal. Biochem.* 395, 231–236. doi: 10.1016/j.ab.2009.07.053

Noctor, G., Reichheld, J. P., and Foyer, C. H. (2018). ROS-related redox regulation and signaling in plants. *Semin. Cell Dev. Biol.* 80, 3–12. doi: 10.1016/j.semcdb.2017.07.013

Olivares, F. L., Baldani, V. L., Reis, V. M., Baldani, J. I., and Döbereiner, J. (1996). Occurrence of the endophytic diazotrophs Herbaspirillum spp. in roots, stems, and leaves, predominantly of Gramineae. *Biol. Fertil. Soils* 21, 197–200. doi: 10.1007/BF00335935

Pieterse, C. M., Zamioudis, C., Berendsen, R. L., Weller, D. M., Van Wees, S. C., and Bakker, P. A. (2014). Induced systemic resistance by beneficial microbes. *Annu. Rev. Phytopathol.* 52, 347–375. doi: 10.1146/annurev-phyto-082712-102340

Queval, G., Hager, J., Gakière, B., and Noctor, G. (2008). Why are literature data for H2O2 contents so variable? A discussion of potential difficulties in the quantitative assay of leaf extracts. *J. Exp. Bot.* 59, 135–146. doi: 10.1093/jxb/erm193

Rajaofera, M. J. N., Wang, Y., Jatoi, Z. A., Jin, P., Cui, H., Lin, C., et al. (2020). Bacillus atrophaeus HAB-5 secretion metabolites preventing occurrence of systemic diseases in tobacco plant. *Eur. J. Plant Pathol.* 156, 159–172. doi: 10.1007/s10658-019-01873-1

Ray, S., Singh, V., Singh, S., Sarma, B. K., and Singh, H. B. (2016). Plant Physiology and Biochemistry Biochemical and histochemical analyses revealing endophytic *Alcaligenes faecalis* mediated suppression of oxidative stress in *Abelmoschus esculentus* challenged with *Sclerotium rolfsii*. *Plant Physiol. Biochem.* 109, 430–441. doi: 10.1016/j.plaphy.2016.10.019

Ruifrok, A. C., and Johnston, D. A. (2001). Quantification of histochemical staining by color deconvolution. *Anal. Quant. Cytol. Histol.* 23, 291–299.

Singh, B. N., and Singh, A. (2011). Trichoderma harzianum - mediated reprogramming of oxidative stress response in root apoplast of sunflower enhances defence against Rhizoctonia solani. *Eur. J. Plant Pathol.* 131, 121–134. doi: 10.1007/s10658-011-9792-4

Singh, R. P., and Jha, P. N. (2017). The PGPR *Stenotrophomonas maltophilia* SBP-9 augments resistance against biotic and abiotic stress in wheat plants. *Front. Microbiol.* 8:1945. doi: 10.3389/fmicb.2017.01945

Ślesak, I., Libik, M., Karpinska, B., Karpinski, S., and Miszalski, Z. (2007). The role of hydrogen peroxide in regulation of plant metabolism and cellular signalling in response to environmental stresses. *Acta Biochim. Polonica* 54, 39–50. doi: 10.18388/abp.2007_3267

Thordal-Christensen, H., Zhang, Z., Wei, Y., and Collinge, D. B. (1997). Subcellular localization of H2O2 in plants. H2O2 accumulation in papillae and hypersensitive response during the barley—powdery mildew interaction. *Plant J.* 11, 1187–1194. doi: 10.1046/j.1365-313X.1997.11061187.x

Torres, M. A., Jones, J. D. G., and Dangl, J. L. (2006). Reactive Oxygen Species Signaling in Response to Pathogens. *Plant Physiol.* 141, 373–378. doi: 10.1104/pp.106.079467

Valencia-Botín, A. J., and Cisneros-López, M. E. (2012). A review of the studies and interactions of *Pseudomonas syringae* pathovars on wheat. *Int. J. Agron.* 2012:692350. doi: 10.1155/2012/692350

Van Breuseguem, F., and Dat, J. F. (2006). Reactive oxygen species in plant cell death. *Plant Physiol.* 141, 384–390. doi: 10.1104/pp.106.078295

Varghese, F., Bukhari, A. B., Malhotra, R., and De, A. (2014). IHC Profiler: an open source plugin for the quantitative evaluation and automated scoring of immunohistochemistry images of human tissue samples. *PLoS One* 9:e96801. doi: 10.1371/journal.pone.0096801

Wang, C. F., Huang, L. L., Buchenauer, H., Han, Q. M., Zhang, H. C., and Kang, Z. S. (2007). Histochemical studies on the accumulation of reactive oxygen species (O2- and H2O2) in the incompatible and compatible interaction of wheat—*Puccinia striiformis* f. sp. tritici. *Physiol. Mol. Plant Pathol.* 71, 230–239. doi: 10.1016/j.pmpp.2008.02.006

Wu, T.-M., Huang, J.-Z., Oung, H.-M., Hsu, Y.-T., Tsai, Y.-C., and Hong, C.-Y. (2019). "H2O2 –based method for rapid detection of transgene-free rice plants from segregating CRISPR / Cas9 genome-edited progenies. *Int. J. Mol. Sci.* 20:3885. doi: 10.3390/ijms20163885